

### Supplementary information

F. J. Martínez-Casado,<sup>\*a</sup> M. Ramos-Riesco,<sup>b</sup> J. A. Rodríguez-Cheda,<sup>b</sup> M. I. Redondo-Yélamos,<sup>b</sup> L. Garrido,<sup>c</sup> A. Fernández-Martínez,<sup>d</sup> J. García-Barriocanal,<sup>e</sup> I. da Silva,<sup>f</sup> M. Durán-Olivencia,<sup>g</sup> A. Poulain.<sup>h</sup>

---

<sup>a.</sup> MAX IV Laboratory, Lund University, Fotongatan 2, SE-225 94 Lund, Sweden. E-mail: francisco.martinez@maxiv.lu.se

<sup>b.</sup> Dpto. Química Física, Facultad de C. Químicas. Universidad Complutense, 28040 Madrid, Spain

<sup>c.</sup> Dpto. Química Física, Instituto de Ciencia y Tecnología de Polímeros, CSIC, 28006 Madrid, Spain

<sup>d.</sup> CNRS & Univ. Grenoble Alpes, ISTerre, F-38041 Grenoble, France

<sup>e.</sup> Univ. Minnesota, Characterization Facility, Minneapolis, MN 55455 USA

<sup>f.</sup> ISIS Facility, Rutherford Appleton Laboratory, Harwell Oxford, Didcot OX11 0QX, United Kingdom

<sup>g.</sup> Department of Chemical Engineering, Imperial College London, United Kingdom

<sup>h.</sup> ESRF, F-38043 Grenoble, France

## 1. Sample preparation

The method of synthesis consists in the metathesis of the potassium ion from the corresponding alkanoate in absolute ethanol solution, by the lead(II) ion, added as nitrate, dissolved in a small amount of water, followed by at least two recrystallizations in benzene.

The chemicals used in the synthesis of lead(II) alkanoates are specified in Table S1.

Table S1. Chemicals used in the synthesis of lead(II) alkanoates

Chemical	Company	Purity (%)
Hexanoic acid	Fluka	≥ 99,5
Heptanoic acid	Fluka	≥ 99
Octanoic acid	Fluka	≥ 99,5
Nonanoic acid	Fluka	≥ 99,5
Decanoic acid	Fluka	≥ 99,5
Undecanoic acid	Fluka	> 97
Dodecanoic acid	Aldrich	≥ 99,5
Tridecanoic acid	Fluka	≥ 98
Tetradecanoic acid	Sigma	≥ 99
Pentadecanoic acid	Sigma	~ 99
Hexadecanoic acid	Fluka	~ 99
Heptadecanoic acid	Fluka	≥ 99
Octadecanoic acid	Merck	~ 99
Potassium hydroxide	Fluka	> 86
Lead(II) nitrate	Merck	> 99,5
Ethanol	Merck	> 99,8
Benzene	Merck	> 99,7

## 2. DSC Calorimetry

**Table S2.** Thermal data (temperatures, enthalpies and entropies) of the transitions of  $\text{Pb}(\text{C9})_2$  and  $\text{Pb}(\text{C10})_2$ .

$\text{Pb}(\text{Cn})_2$	Transition	T / K	$\Delta_{\text{trs}}H / \text{kJ}\cdot\text{mol}^{-1}$	$\Delta_{\text{trs}}S / \text{J}\cdot\text{K}^{-1}\cdot\text{mol}^{-1}$
$\text{Pb}(\text{C9})_2$	$\text{SII}$ (polymorph B)- $\text{SI}$ ( <sup>a</sup> )	$347.3 \pm 0.4$	$27.91 \pm 0.4$	$80.4 \pm 1.1$
	$\text{SII}$ (polymorph A)- $\text{SI}$ ( <sup>b</sup> )	$354.2 \pm 0.3$	$7.540 \pm 0.2$	$21.3 \pm 0.5$
	$\text{SI-LC}$	$371.6 \pm 0.4$	$16.6 \pm 0.2$	$44.6 \pm 0.5$
	$\text{LC-IL}$	$387.9 \pm 0.5$	$0.97 \pm 0.07$	$2.5 \pm 0.2$
$\text{Pb}(\text{C10})_2$	$\text{SII}$ (polymorph B)- $\text{SI}$ ( <sup>a,c</sup> )	$355.5 \pm 0.2$	$33.6 \pm 1.0$	$94.6 \pm 3.0$
	$\text{SII}$ (polymorph A)- $\text{SI}$ ( <sup>d</sup> )	$358.3 \pm 0.4$	$33.1 \pm 0.7$	$92.5 \pm 2.0$
	$\text{SI-LC}$	$369.4 \pm 0.2$	$17.4 \pm 0.9$	$47.0 \pm 2.4$
	$\text{LC-IL}$	$386.3 \pm 0.3$	$1.04 \pm 0.03$	$2.7 \pm 0.1$

<sup>a</sup> Transition in two steps. <sup>b</sup> Measured in the second heating from a 9:1 mixture of polymorphs A and B (from XRD data) (after cooling at  $2 \text{ K}\cdot\text{min}^{-1}$ ). <sup>c</sup> Enthalpy estimated from a 15:85 mixture (A:B). <sup>d</sup> Measured in the second heating.

\*\* Although the  $\text{SII}$  (polymorph B)-  $\text{SI}$  transition occurs in two steps it was not possible to determine the structure of the intermediate species by XRD (due to the measurement limitation in this short temperature range).

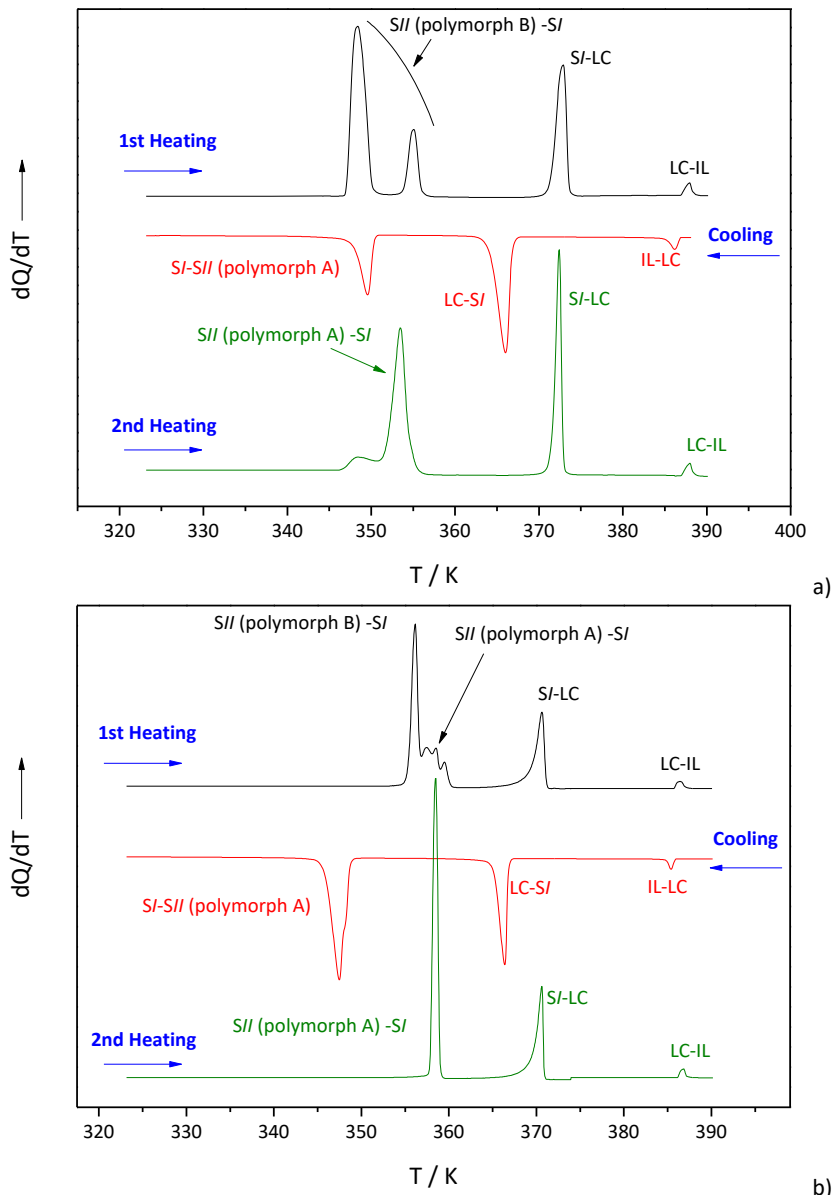


**Fig. S1.** DSC Thermograms (recorded at  $1\text{K}\cdot\text{min}^{-1}$ ) of  $\text{Pb}(\text{C9})_2$  and  $\text{Pb}(\text{C10})_2$ , indicating the transitions in the first and second heatings and the cooling.

**Table S3.** Thermal data (temperatures, enthalpies and entropies) of the transitions of the rest of the members of lead(II) alkanoates series. SII corresponds to the polymorphic form A from Pb(C2)<sub>2</sub> ( $\beta$ ) to Pb(C8), and to B from Pb(C11)<sub>2</sub> to Pb(C18).

Pb(Cn) <sub>2</sub>	Transition	T / K	$\Delta_{trs}H / \text{kJ}\cdot\text{mol}^{-1}$	$\Delta_{trs}S / \text{J}\cdot\text{K}^{-1}\cdot\text{mol}^{-1}$
Pb(C2) <sub>2</sub> <sup>a</sup>	S( $\alpha$ )-S( $\beta$ )	335.1 $\pm$ 0.3	1.6 $\pm$ 0.2	4.8 $\pm$ 0.6
	S( $\beta$ )-IL	480.3 $\pm$ 0.3	12.9 $\pm$ 0.2	26.9 $\pm$ 0.4
Pb(C3) <sub>2</sub> <sup>b</sup>	SII-IL	398.2 $\pm$ 0.4	13.1 $\pm$ 0.1	32.9 $\pm$ 0.3
Pb(C4) <sub>2</sub> <sup>b</sup>	SII-IL	346.5 $\pm$ 0.3	14.7 $\pm$ 0.1	42.4 $\pm$ 0.3
	S/*-IL	322.8 $\pm$ 0.5	7.7 $\pm$ 0.4	32 $\pm$ 2
Pb(C5) <sub>2</sub> <sup>c</sup>	SII-SI	328.2 $\pm$ 0.6	8.8 $\pm$ 0.1	26.8 $\pm$ 0.4
	SI-IL	355.6 $\pm$ 0.3	12.6 $\pm$ 0.1	35.3 $\pm$ 0.3
Pb(C6) <sub>2</sub> <sup>b</sup>	SII-LC	339.3 $\pm$ 0.1	22.6 $\pm$ 0.1	66.6 $\pm$ 0.3
	LC-IL	354.2 $\pm$ 0.2	1.2 $\pm$ 0.1	3.4 $\pm$ 0.3
	S/*-IL	332.8 $\pm$ 0.4	(#)	
Pb(C7) <sub>2</sub> <sup>b</sup>	SII-SI	344.1 $\pm$ 0.1	16.5 $\pm$ 0.1	48.0 $\pm$ 0.3
	SI-LC (§)	355.9 $\pm$ 0.3	12.9 $\pm$ 0.1	36.2 $\pm$ 0.3
	LC-IL	372.9 $\pm$ 0.2	1.3 $\pm$ 0.1	3.5 $\pm$ 0.3
Pb(C8) <sub>2</sub>	SII-SI	346.4 $\pm$ 0.1	24.0 $\pm$ 0.2	69.4 $\pm$ 0.6
	SI-LC	350.6 $\pm$ 0.1	10.5 $\pm$ 0.2	29.8 $\pm$ 0.6
	LC-IL	384.4 $\pm$ 0.1	1.2 $\pm$ 0.1	3.2 $\pm$ 0.3
Pb(C11) <sub>2</sub>	SII-SI	360.8 $\pm$ 0.2	40.4 $\pm$ 0.2	111.9 $\pm$ 0.6
	SI-LC	377.2 $\pm$ 0.2	21.9 $\pm$ 0.1	58.2 $\pm$ 0.3
	LC-IL	390.1 $\pm$ 0.1	0.9 $\pm$ 0.1	2.4 $\pm$ 0.1
Pb(C12) <sub>2</sub>	SII-SI	367.0 $\pm$ 0.2	49.7 $\pm$ 0.1	135.3 $\pm$ 0.3
	SI-LC	377.5 $\pm$ 0.1	27.6 $\pm$ 0.2	73.2 $\pm$ 0.5
	LC-IL	384.5 $\pm$ 0.1	1.0 $\pm$ 0.1	2.5 $\pm$ 0.1
Pb(C13) <sub>2</sub>	SII-SI	372.4 $\pm$ 0.1	51.7 $\pm$ 0.2	138.8 $\pm$ 0.6
	SI-IL	382.5 $\pm$ 0.1	33.2 $\pm$ 0.2	86.8 $\pm$ 0.5
Pb(C14) <sub>2</sub>	SII-SI	373.2 $\pm$ 0.1	55.2 $\pm$ 0.2	147.9 $\pm$ 0.6
	SI-IL	383.3 $\pm$ 0.2	37.3 $\pm$ 0.2	97.4 $\pm$ 0.5
Pb(C15) <sub>2</sub>	SII-SI	376.1 $\pm$ 0.2	59.7 $\pm$ 0.2	158.6 $\pm$ 0.6
	SI-IL	385.4 $\pm$ 0.1	41.5 $\pm$ 0.3	107.7 $\pm$ 0.5
Pb(C16) <sub>2</sub>	SII-SI	377.8 $\pm$ 0.1	67.5 $\pm$ 0.1	178.6 $\pm$ 0.3
	SI-IL	385.0 $\pm$ 0.1	50.4 $\pm$ 0.1	130.9 $\pm$ 0.3
Pb(C17) <sub>2</sub>	SII-SI	382.3 $\pm$ 0.1	69.3 $\pm$ 0.1	181.3 $\pm$ 0.3
	SI-IL	387.6 $\pm$ 0.1	54.4 $\pm$ 0.2	140.3 $\pm$ 0.6
Pb(C18) <sub>2</sub>	SII-SI	383.6 $\pm$ 0.1	74.0 $\pm$ 0.3	192.8 $\pm$ 0.8
	SI-IL	388.8 $\pm$ 0.2	56.5 $\pm$ 0.2	145.2 $\pm$ 0.5

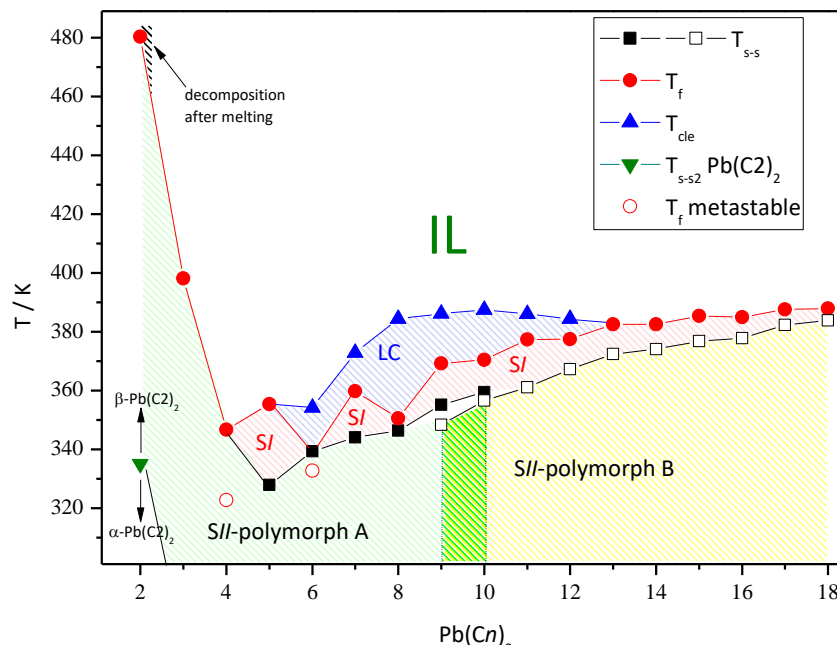
(\*) metastable phase; (§) fusion in two steps (ref 1); (#) Not measurable enthalpy (metastable transition). <sup>a</sup> From reference 2, <sup>b</sup> from reference 3, and <sup>c</sup> from reference 4

1 A. Sánchez Arenas, M. V. García Pérez, M. I. Redondo-Yélamos, J. A. Rodríguez Cheda, M. V. Roux and C. Turrión, *Liq. Cryst.* 1995, **18**, 431.

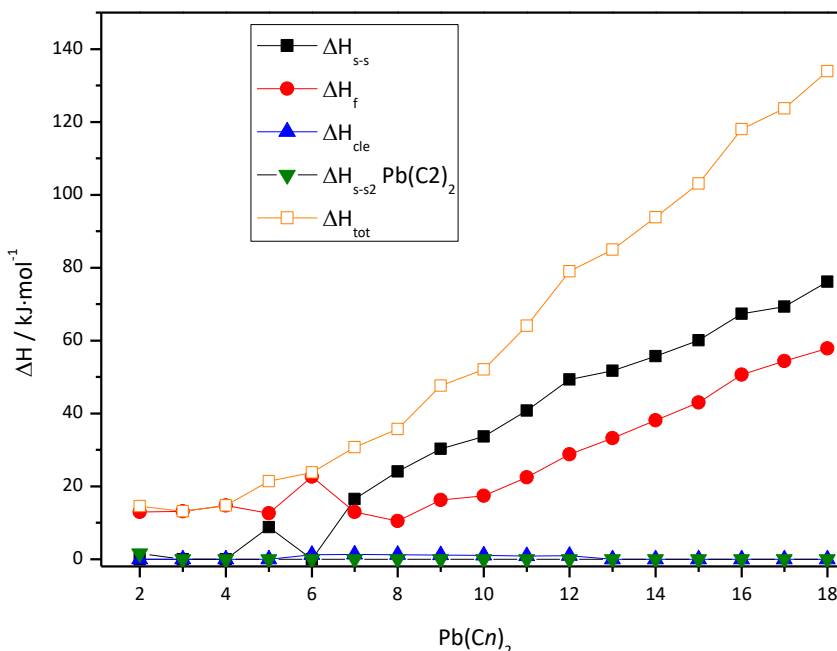
2 F. J. Martínez-Casado, M. Ramos-Riesco, J. A. Rodríguez -Cheda, F. Cucinotta, E. Matesanz, I. Miletto, E. Gianotti and L. Marchese, *Inorg. Chem.* 2016, **55**, 8576.

3 F. J. Martínez Casado, M. Ramos-Riesco, J. A. Rodríguez-Cheda, F. Cucinotta, A. Fernández-Martínez, L. Garrido, E. Matesanz and L. Marchese, *J. Mater. Chem. C*, 2014, **15**, 497.

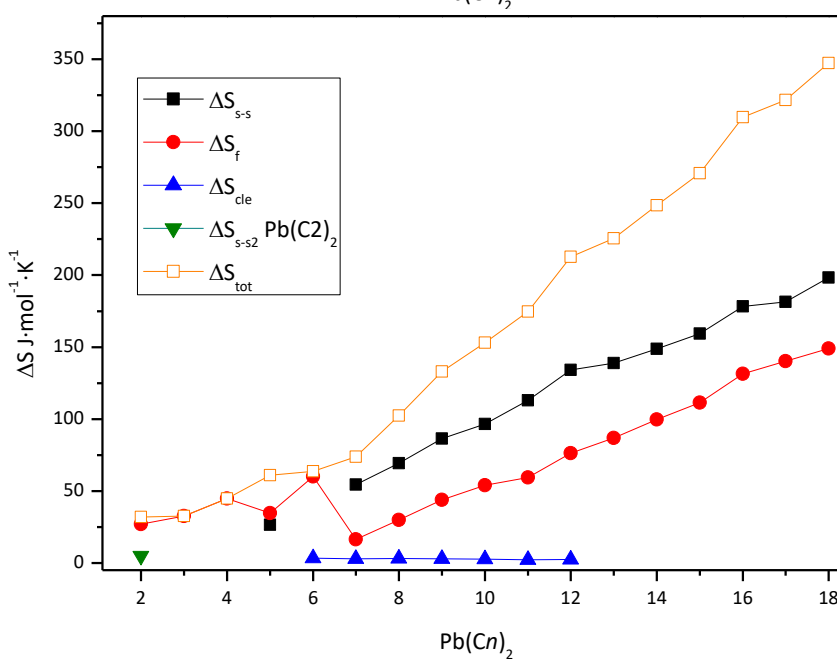
4 F. J. Martínez Casado, M. Ramos Riesco, A. Sánchez Arenas, M. V. García Pérez, M. I. Redondo-Yélamos, S. López-Andrés, L. Garrido and J. A. Rodríguez Cheda, *J. Phys. Chem. B* 2008, **112**, 16601.



a)



b)



c)

**Fig. S2.** Temperature, Enthalpy and Entropy vs. number of C atoms in the  $\text{Pb}(\text{C}_n)_2$  series. The enthalpy and entropy data are referred to the stable polyform in the SII phase (A from  $\text{Pb}(\text{C}_2)_2$  ( $\text{S}\beta$ ) to  $\text{Pb}(\text{C}_8)$ , and to B from  $\text{Pb}(\text{C}_9)_2$  to  $\text{Pb}(\text{C}_{18})$ .

### 3. High Resolution Powder Diffraction (HRPD)

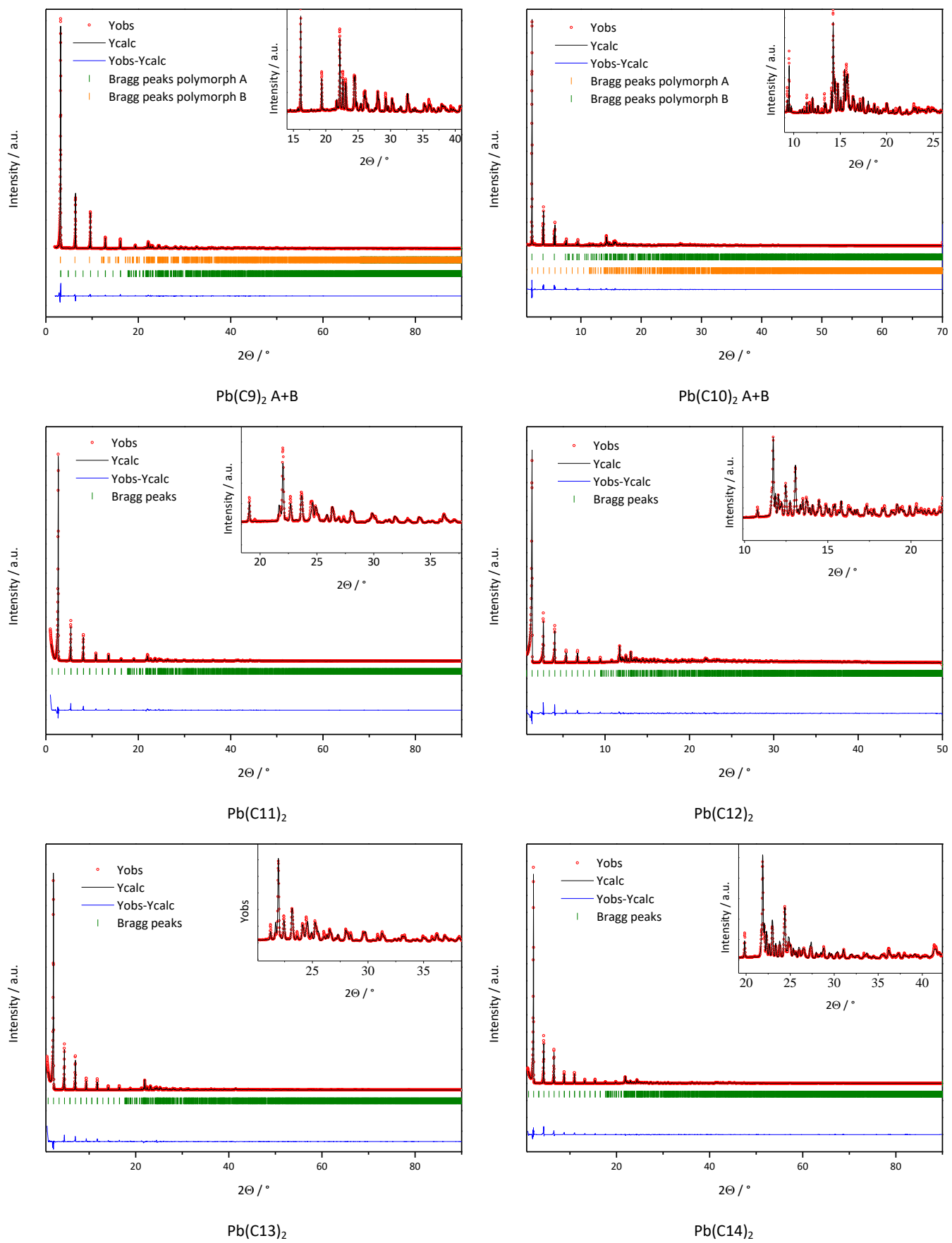


**Fig. S3.** Rietveld refinement for Pb(C9)<sub>2</sub> (mixture of polymorphs A and B), Pb(C10)<sub>2</sub> (mixture of A and B), Pb(C11)<sub>2</sub>, Pb(C12)<sub>2</sub>, Pb(C13)<sub>2</sub> and Pb(C14)<sub>2</sub>.

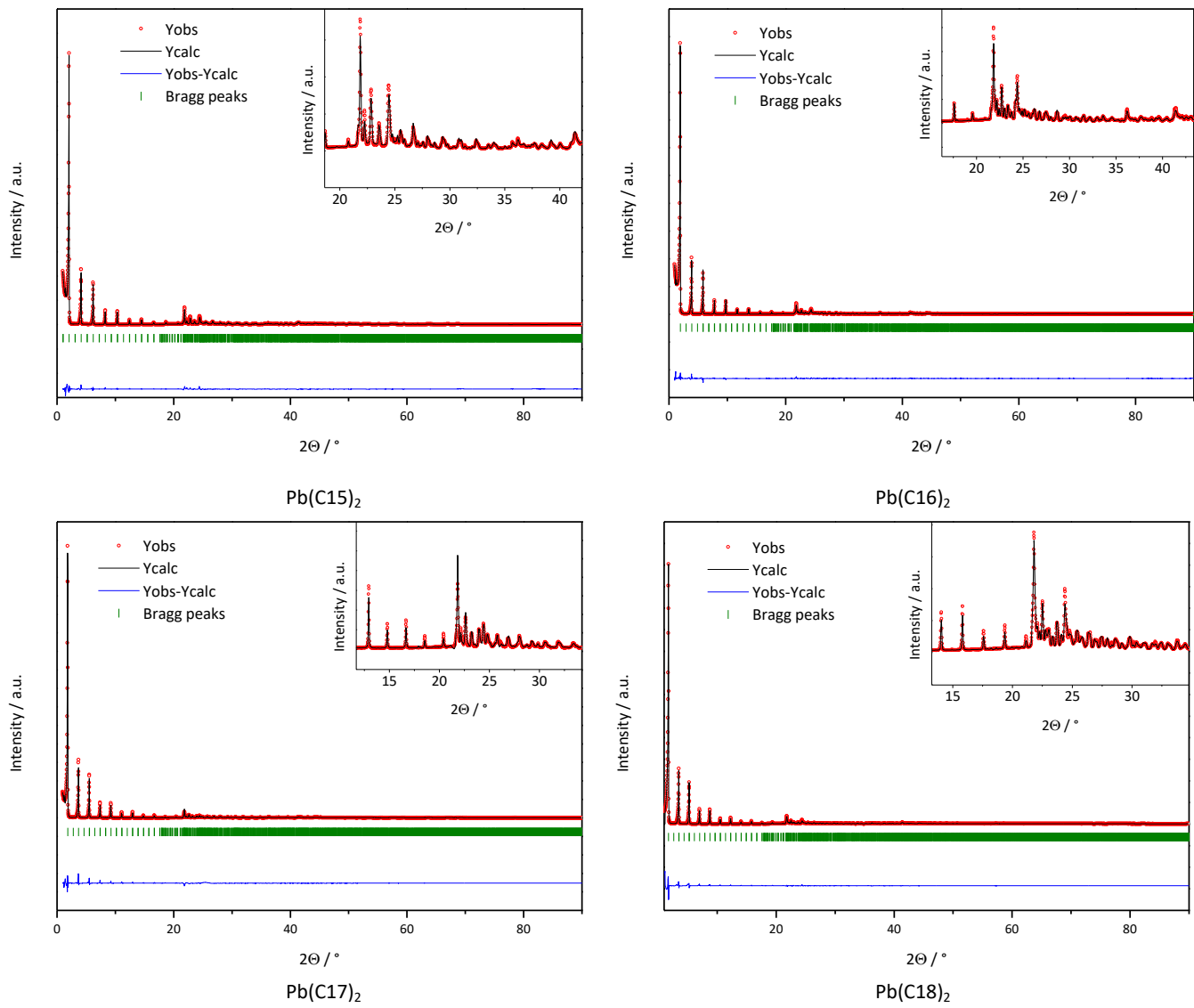


**Fig. S4.** Rietveld refinement for  $\text{Pb}(\text{C}14)_2$ ,  $\text{Pb}(\text{C}15)_2$ ,  $\text{Pb}(\text{C}16)_2$ ,  $\text{Pb}(\text{C}17)_2$  and  $\text{Pb}(\text{C}18)_2$ .

**Table S4.** Pb-O and Pb-Pb distances for  $\text{Pb}(\text{C}10)_2\text{-A}$  and  $\text{Pb}(\text{C}10)_2\text{-B}$  (at 298 K). obtained from the SCXRD data.

Compound	Atom 1	Atom 2	Count	Distance / Å
$\text{Pb}(\text{C}10)_2\text{-A}$	Pb1	O1	1x	2.4209(50)
		O2	1x	2.4487(54)
		O4	1x	2.5752(54)
		O4	1x	2.5765(56)
		O3	1x	2.6178(55)
		O3	1x	2.7212(59)
		O2	1x	3.0186(55)
	Pb1	Pb1	1x	4.3374(23)
		Pb1	1x	4.3637(23)
		Pb1	2x	4.910(5)
		Pb1	1x	5.0012(26)
		Pb1	1x	5.0545(27)
$\text{Pb}(\text{C}10)_2\text{-B}$	Pb1	O2	1x	2.4345(439)
		O3	1x	2.5004(531)
		O1	1x	2.5866(441)
		O3	1x	2.5943(507)
		O1	1x	2.6378(432)
		O4	1x	2.8449(505)
		O4	1x	2.9069(500)
	Pb1	Pb1	2x	4.3014(46)
		Pb1	2x	4.5021(47)
		Pb1	2x	4.9810(61)

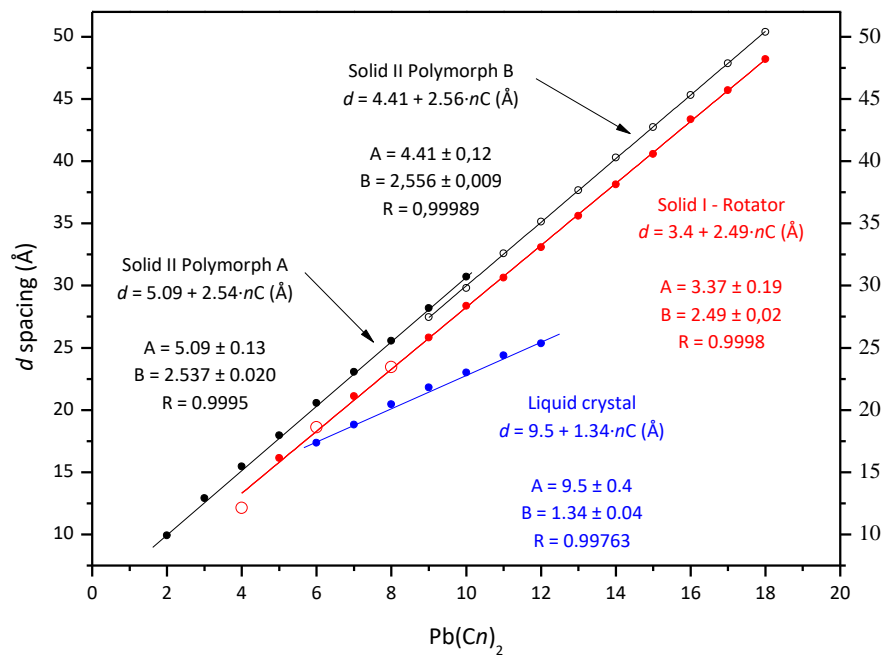


**Fig. S5.**  $d$ -spacing values for the different phases of the members of the lead(II) alkanoates series

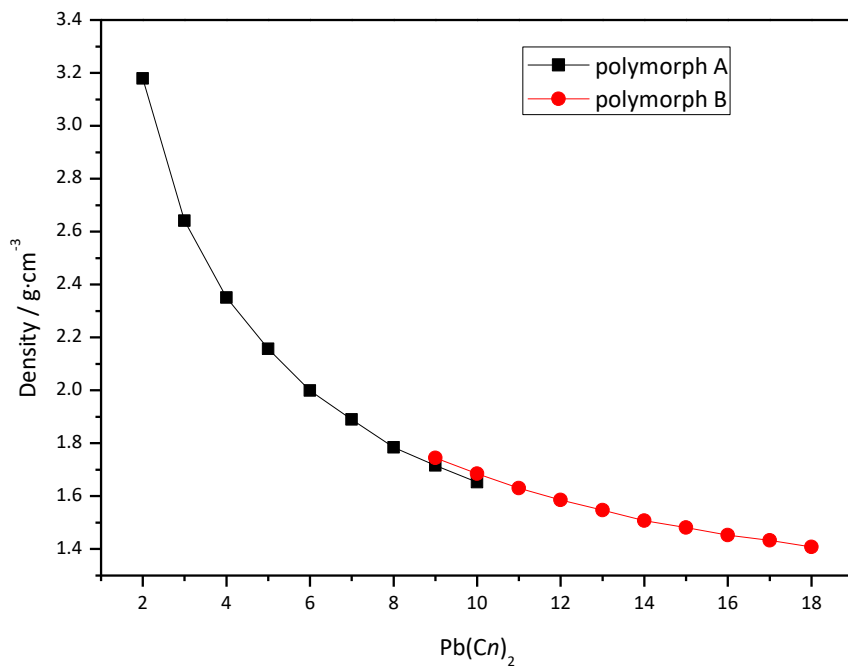


**Fig. S6.** Density of the different polymorphs of the lead(II) alkanoates series in the SII phase.

**Table S5.** Unit cell parameters ( $a$ ,  $b$ ,  $c$  and  $\beta$ ) for the monoclinic cells obtained by the DICVOL06 program for the *S/I* phase of the following members of the lead(II) series, and figures of merit (M and F) using N peaks.

Compound	$a / \text{\AA}$	$b / \text{\AA}$	$c / \text{\AA}$	$\beta / {}^\circ$	M(N)	F(N)	N
Pb(C10) <sub>2</sub>	8.52	14.92	28.79	98.64	13.9	55.2	26
Pb(C11) <sub>2</sub>	8.55	14.89	31.25	97.98	10.0	45.0	28
Pb(C12) <sub>2</sub>	8.52	14.90	33.77	97.16	19.1	116.7	33
Pb(C13) <sub>2</sub>	8.53	14.87	36.20	96.65	20.8	100.9	23
Pb(C14) <sub>2</sub>	8.52	14.88	38.65	96.18	16.2	80.5	30
Pb(C15) <sub>2</sub>	8.54	14.87	41.15	95.83	14.9	83.6	30
Pb(C16) <sub>2</sub>	8.52	14.87	43.62	95.48	10.4	50.1	29
Pb(C17) <sub>2</sub>	8.53	14.85	46.08	95.33	27.7	180.4	27

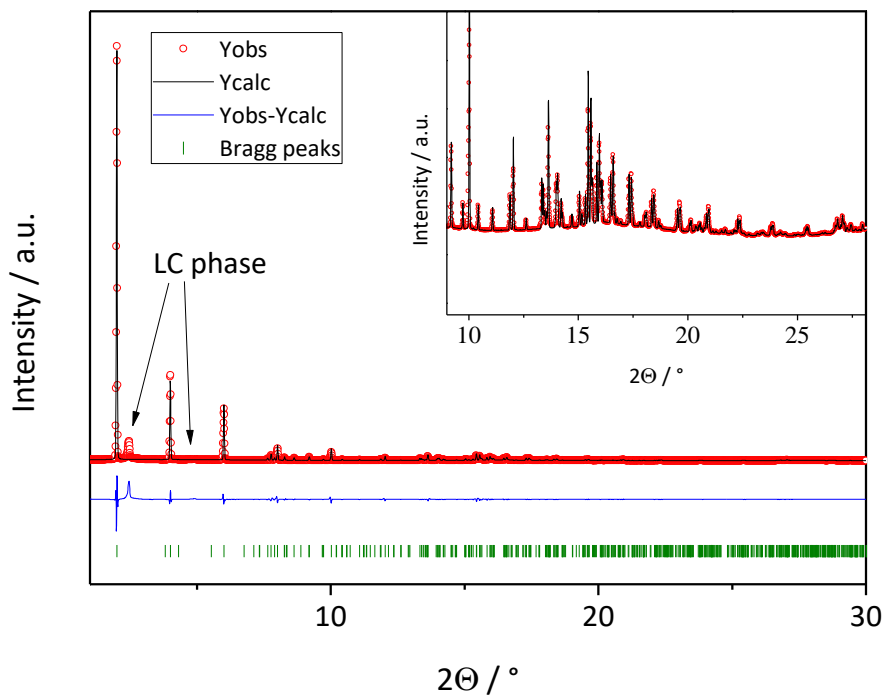


**Fig. S7.** Profile matching for Pb(C10)<sub>2</sub> in the *S/I* phase, showing the good agreement of the fit and the presence of two peaks corresponding to the LC phase.

#### 4. FTIR

The room temperature infrared spectra of lead soaps show the characteristic features of the alkyl chain plus bands corresponding to the carboxylate vibrational modes. In the crystal phase (SII), the  $\text{CH}_3$  asymmetric stretching band split in two components at 2955 and  $2960\text{ cm}^{-1}$  for all the compounds. At the SII to SI transition temperature only one the band at  $2960\text{ cm}^{-1}$  is observed for this mode indicating that from this point free rotation of the methyl groups takes place. The  $\text{CH}_2$  symmetric ( $\nu_{\text{symm}}$ ) and asymmetric ( $\nu_{\text{asymm}}$ ) stretching bands at  $2849\text{ cm}^{-1}$  and  $2918\text{ cm}^{-1}$  respectively shift to  $2855$  and  $2826\text{ cm}^{-1}$  in the rotator solid. This shifting to higher frequencies is characteristic of the presence of gauche disorder in the alkyl chain.

The carboxylate asymmetric stretching band appears as a doublet at room temperature but transforms in a unique band at a temperature coincident with that of the SII to SI phase transition. An abrupt frequency shift of both asymmetric and symmetric COO<sup>-</sup> is observed at the SII (in both polymorphs) to SI transition temperature in all of the compounds, proving that changes in the coordination of the carboxylate group to the Pb(II) have taken place at this transition (see Figures S8-S10). Moreover, the crystal field splitting observed when  $n > 9$  in the  $\text{CH}_2$  scissoring (around  $1465\text{ cm}^{-1}$ ) and rocking (around  $720\text{ cm}^{-1}$ ) modes also disappears at this temperature. These facts, point to a polymorphic change to a more disordered solid (the *all-trans* carbon planes start to rotate) taking place at this temperature. In addition, very weak bands ascribed to localized *gtg* (*kink*) sequences at  $1306\text{ cm}^{-1}$  and end gauche defects at about  $1340\text{ cm}^{-1}$  can be observed. These bands correspond to kink defects appearing in the alkyl chain as consequence of methylene rotational movements taking place at the solid transition temperature.

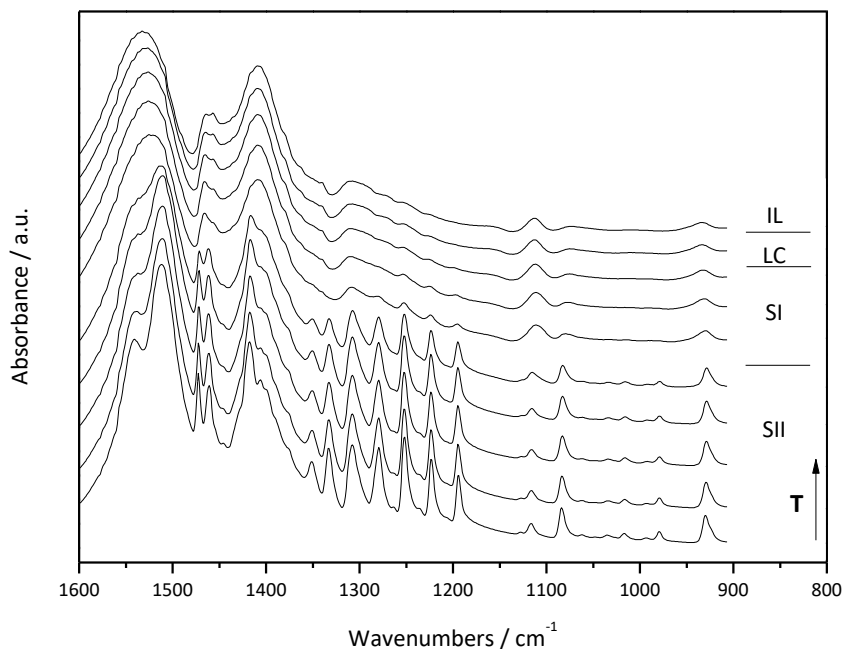


**Fig. S8.** FTIR spectra of  $\text{Pb}(\text{C14})_2$ , at 298, 313, 333, 353, 368, 373, 378 and 393 K, showing the different phases (SII, SI and IL).

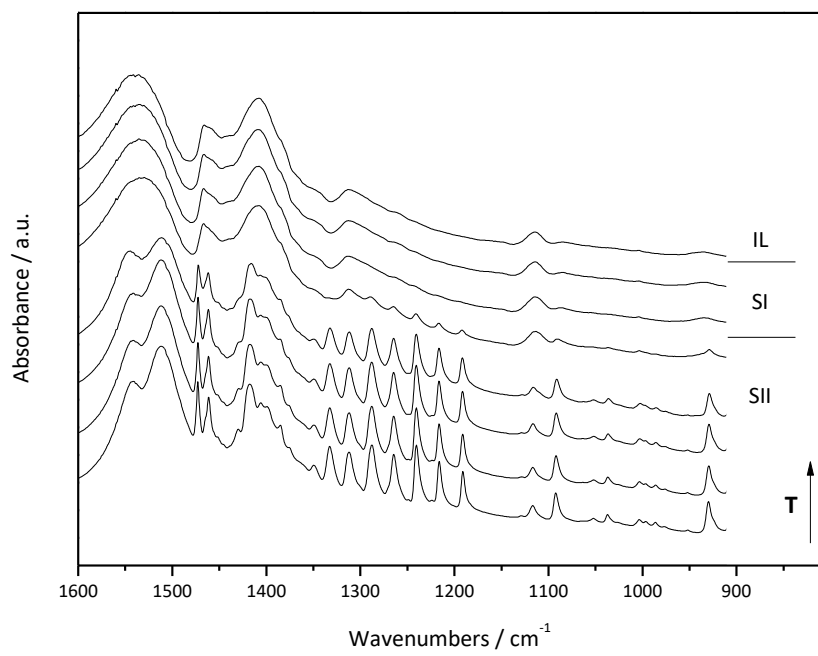


**Fig. S9.** FTIR spectra of  $\text{Pb}(\text{C14})_2$ , at 298, 313, 333, 353, 368, 373, 378 and 393 K, showing the different phases (SII, SI and IL).

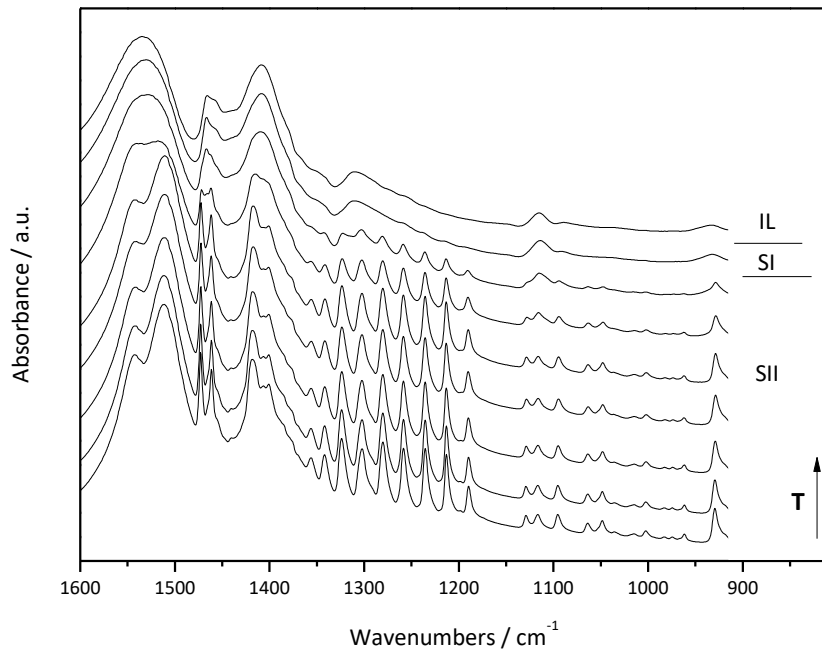


**Fig. S10.** FTIR spectra of  $\text{Pb}(\text{C15})_2$ , at 298, 313, 333, 343, 353, 368, 373, 378 and 393 K, showing the different (SII, SI and IL).

## 5. PDF Analysis

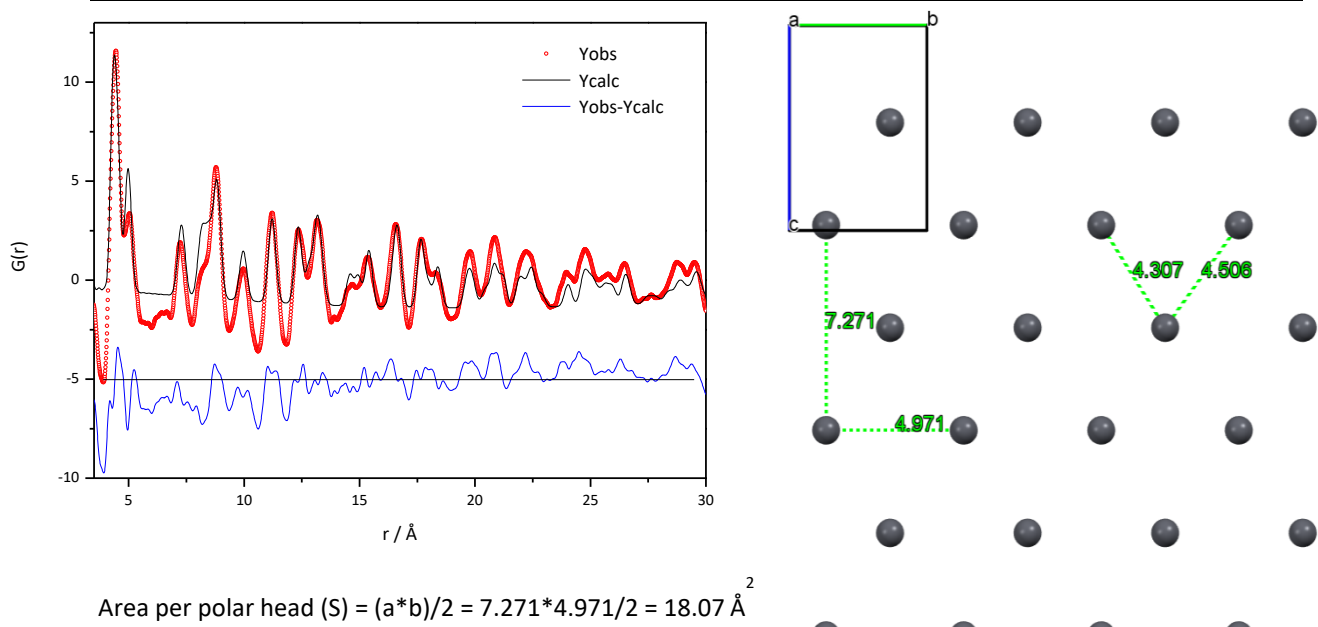


**Fig. S11.** Fitting SII phase ( $\text{Pb}(\text{C11})_2$ , polymorph B) with PDFgui, using only Pb atoms and without modifying the crystallographic data obtained XRD

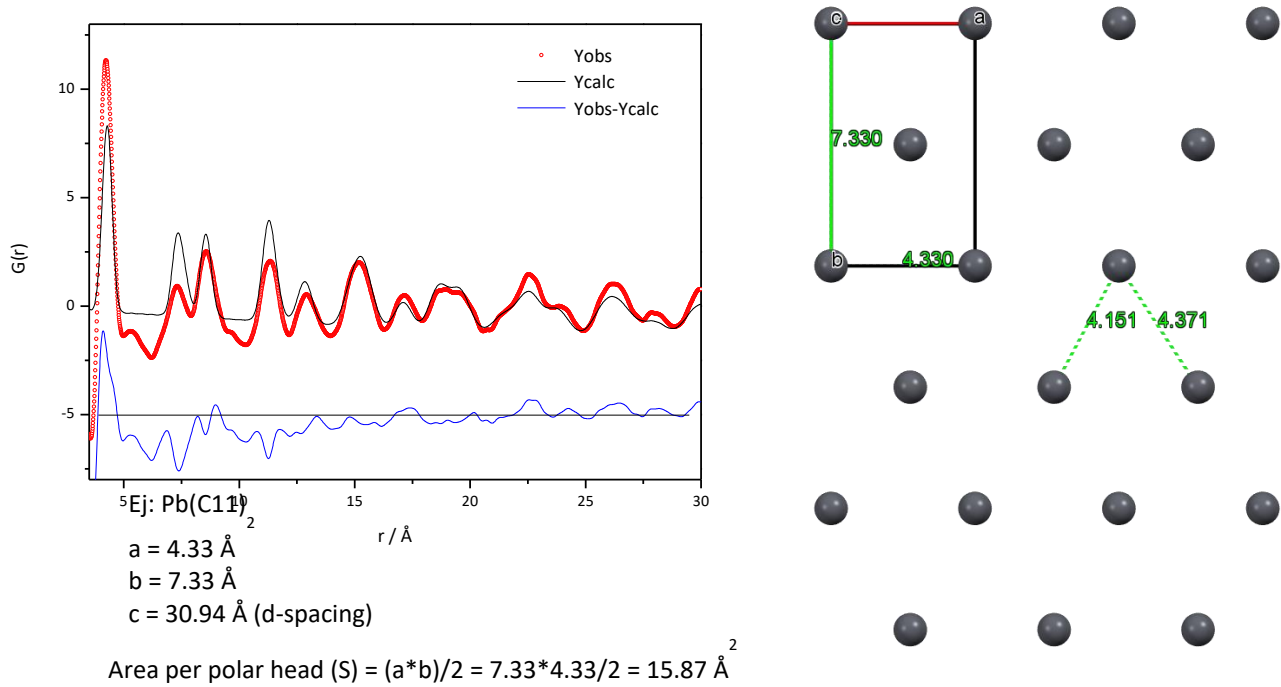


**Fig. S12.** Simulation S/I phase ( $\text{Pb}(\text{C11})_2$ ), refining the  $a$  and  $b$  parameters and the position of one Pb atom in the XY plane (the other one fixed in the origin: 0,0,0).

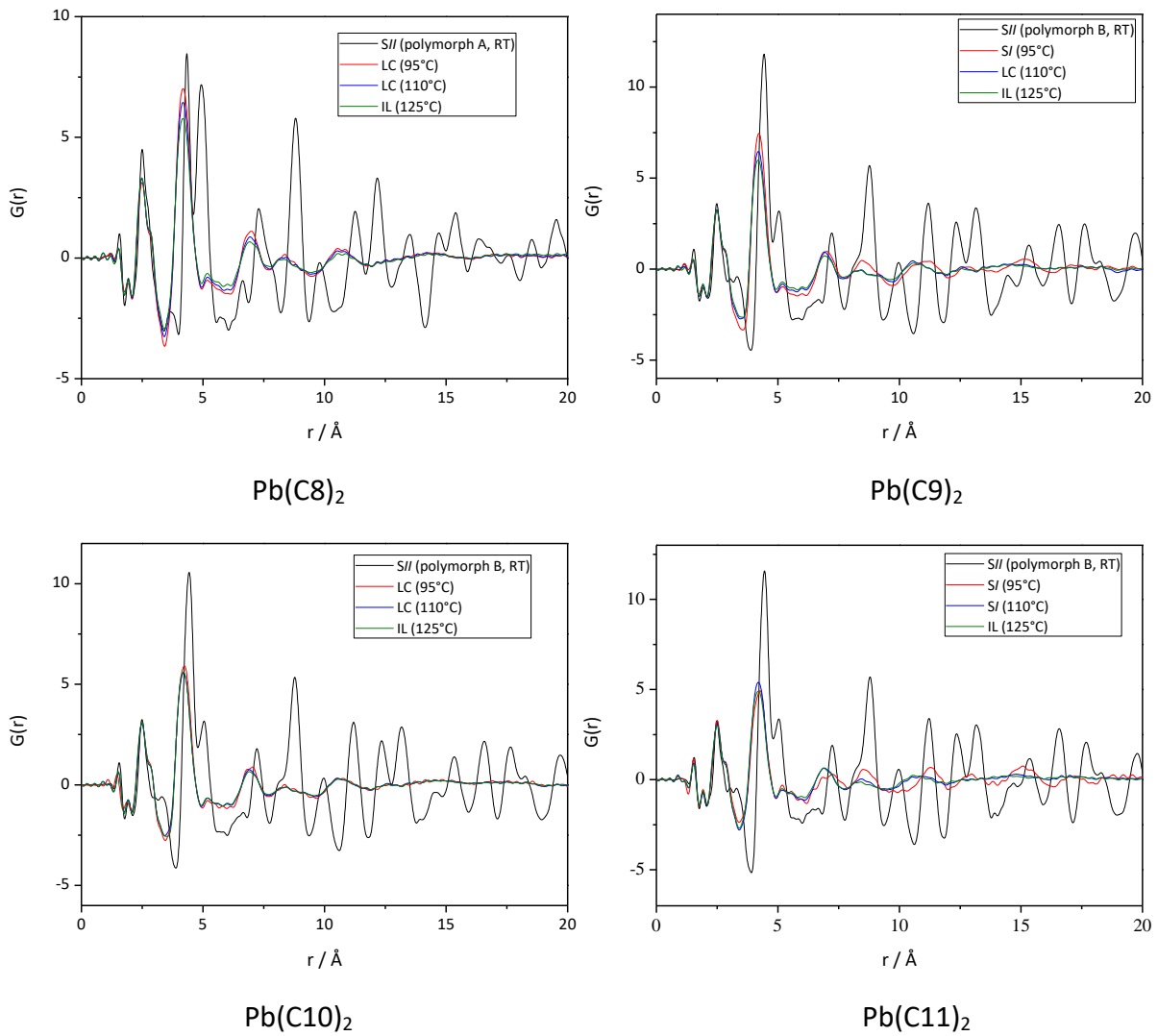


**Fig. S12.** PDF analysis for the different phases of  $\text{Pb}(\text{C8})_2$  to  $\text{Pb}(\text{C11})_2$ : crystal phase at RT ( $\text{SII}$ , polymorph B), intermediate solid phase ( $\text{SI}$ ), liquid crystal (LC) and liquid phase (IL).

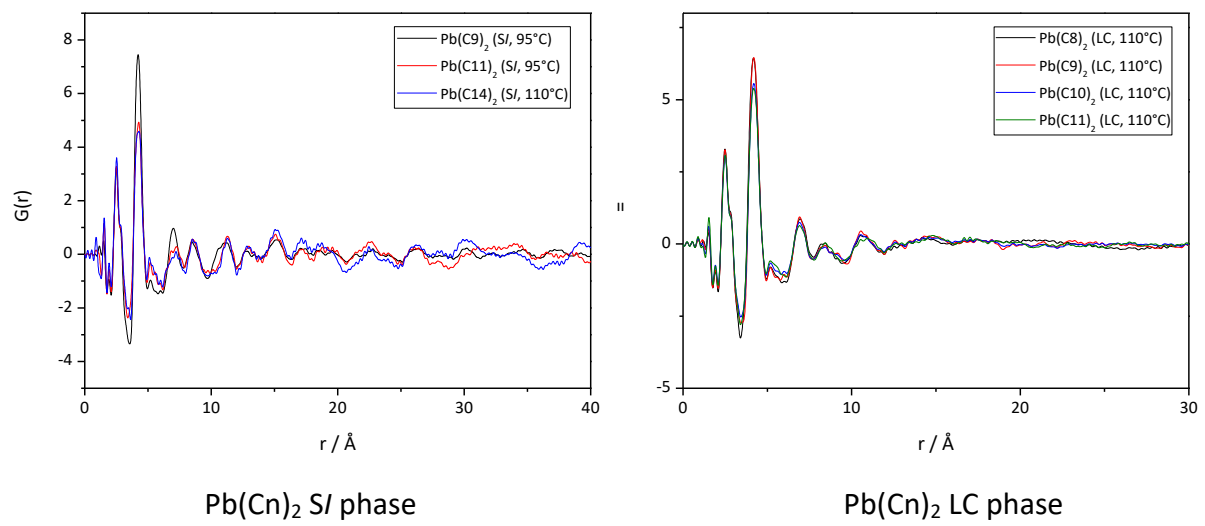


**Fig. S13.** PDF analysis for the SI phase and the LC phase for different compounds of the series.

**PDF on texturized samples (Figures S14 and S15):**

Due to the layered structure of these compounds, they may present preferred orientation. The 1 mm capillaries used for the PDF measurements were not rotated (rotation helps randomizing the orientation of crystal domains). In some capillaries for some compounds, preferred orientation was clearly observed and, in those cases, partial PDFs or “pseudo-PDFs” integrating different sections of the 2D images. Thus, the signals in the different directions can be enhanced.

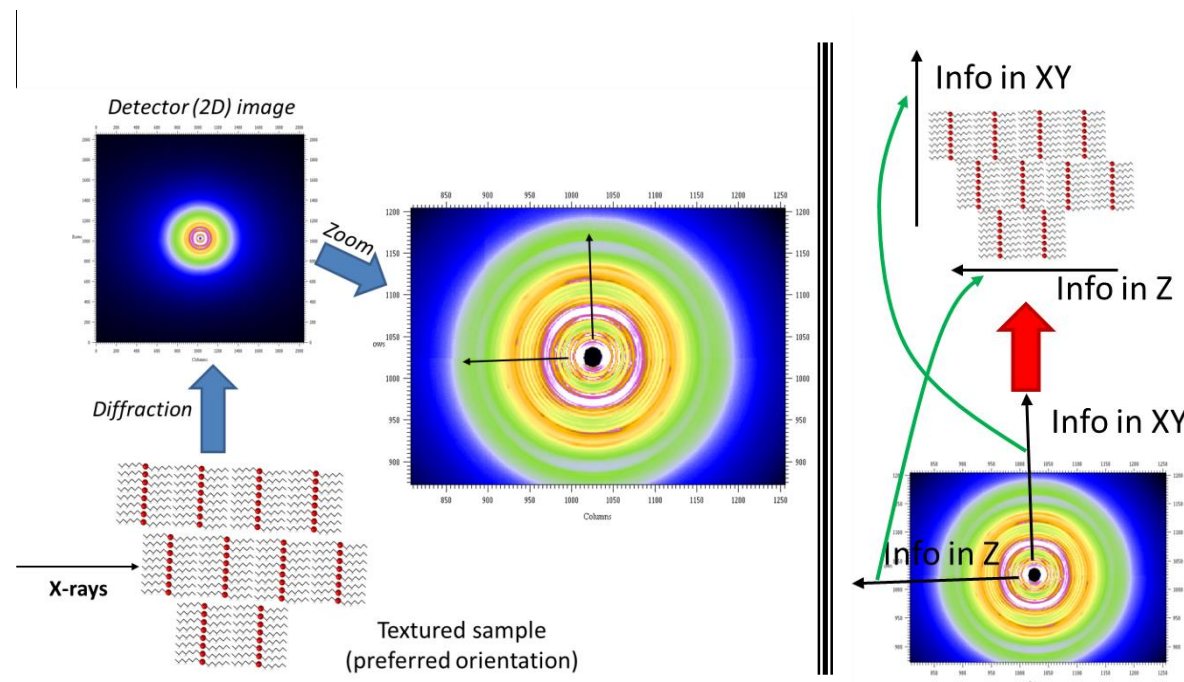


**Fig. S14.** Diffraction signal of a textured sample on a 2D detector.

This was carried out to compare the pseudo-PDF signal in plane (XY) and out of the plane (Z) of different compounds ( $\text{Pb}(\text{C11})_2$  and  $\text{Pb}(\text{C14})_2$ ) in the S/I phase. In this sense, similar signal is observed in the pseudo-PDF in the plane (XY), independently of the alkyl chain. On the other hand, in the out of plane signal, the interlayer  $d$ -spacing can be clearly observed (see Figure S16).

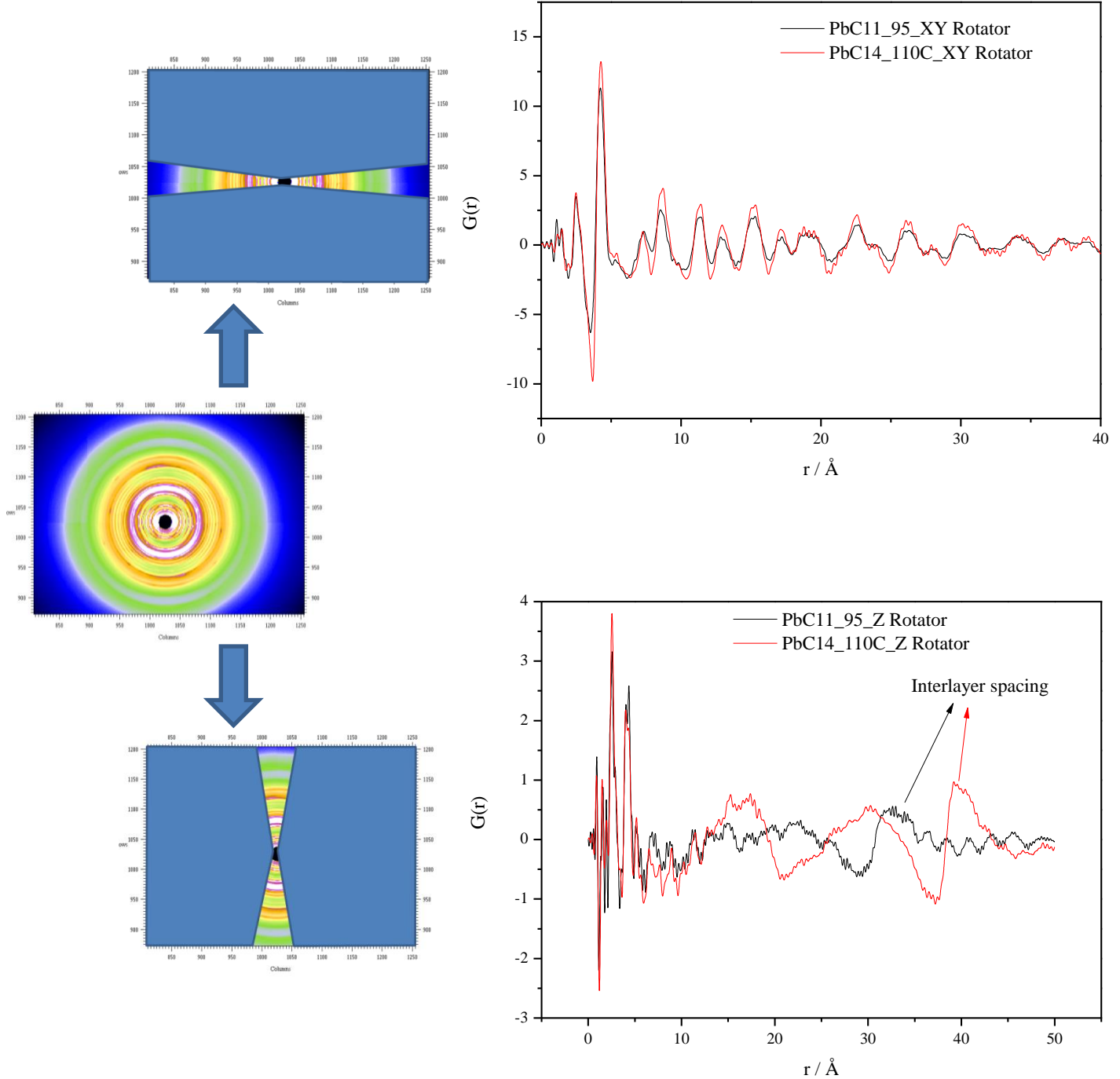


**Fig. S15.** Partial PDFs or “pseudo-PDFs” for  $\text{Pb}(\text{C}11)_2$  and  $\text{Pb}(\text{C}14)_2$  in plane (XY) and out of the plane (Z), obtained from the integration of different sections (“cakes”) of the 2D images.

## 6. Electric spectroscopy

Cylindrical pellets 12 mm in diameter and 1 mm thick were prepared for electrical measurements and silver electrodes (7 mm diameter) were painted at both faces. Electric Spectroscopy measurements were performed by using an LCR meter HP 4284A, in the frequency range 100 Hz - 1 MHz. Samples were placed in a quartz cell, and temperature was varied between 30 °C and 115 °C. Special care was taken to keep the thermal equilibrium of the sample, using slow heating and cooling rates of 0.5 K·min<sup>-1</sup>.

A significant increase in the electrical conductivity from the SII to the SI phase is observed in the long members of the lead(II) alkanoates series.

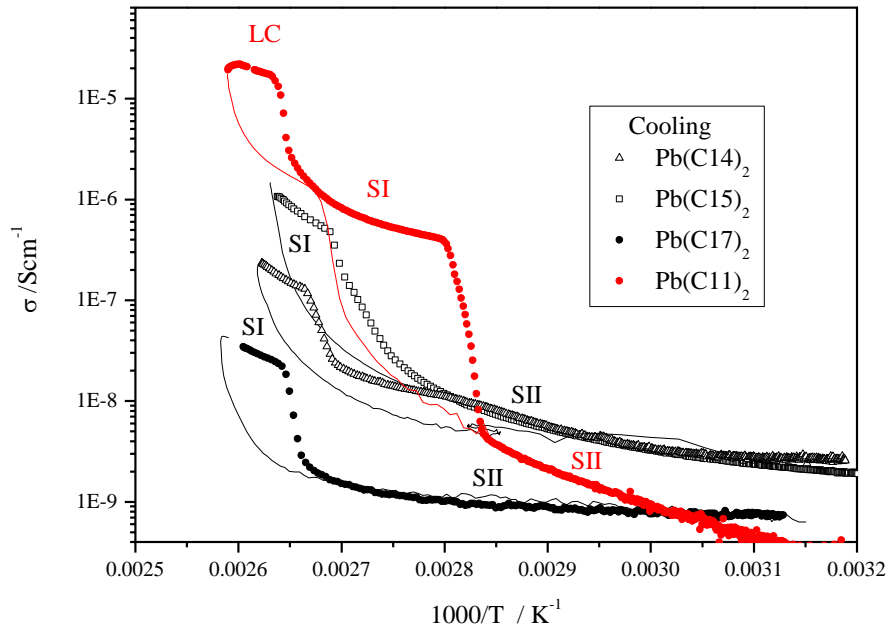


**Fig. S16.** Electrical conductivity as a function of temperature on heating (-) and cooling for  $\text{Pb}(\text{C}14)_2$ ,  $\text{Pb}(\text{C}15)_2$ , and  $\text{Pb}(\text{C}17)_2$  ( $\triangle$ ,  $\square$ , and  $\diamond$ , respectively) at 1 kHz. The measurement for  $\text{Pb}(\text{C}11)_2$  (from reference 5) is included for comparison.

## 7. C-13 and Pb-207 solid state NMR

### NMR measurements of Pb(II) alkanoates.

All NMR measurements were performed according to the experimental procedure described in F.J. Martínez Casado et al., *J. Phys. Chem. B* **2008**, 112, 16601. The only parameter changed was the temperature at which the second NMR measurement was performed. Thus, this temperature was set to an intermediate value between the first two thermal transitions exhibited by the corresponding alkanoate (see Table S5).

**Table S6.** Values of temperature used in NMR measurements.\*

Compound	T, K 1 <sup>st</sup> NMR exp.	T, K 2 <sup>nd</sup> NMR exp.	T <sub>s-sr</sub> K (crystal-rotator)
Pb(C10) <sub>2</sub>	296.5 (1)	364.9 (1.4)	359.4
Pb(C11) <sub>2</sub>	296.5 (1)	369.0 (1.4)	361.1
Pb(C14) <sub>2</sub>	296.5 (1)	379.5 (1.4)	374.1
Pb(C15) <sub>2</sub>	296.5 (1)	381.2 (1.4)	376.8

\*maximum deviation from the mean in parenthesis

\* Summary, NMR measurements corresponding to Pb(II) decanoate:

<sup>13</sup>C CP-MAS, HPPD  
sp. rate: 6.5 kHz

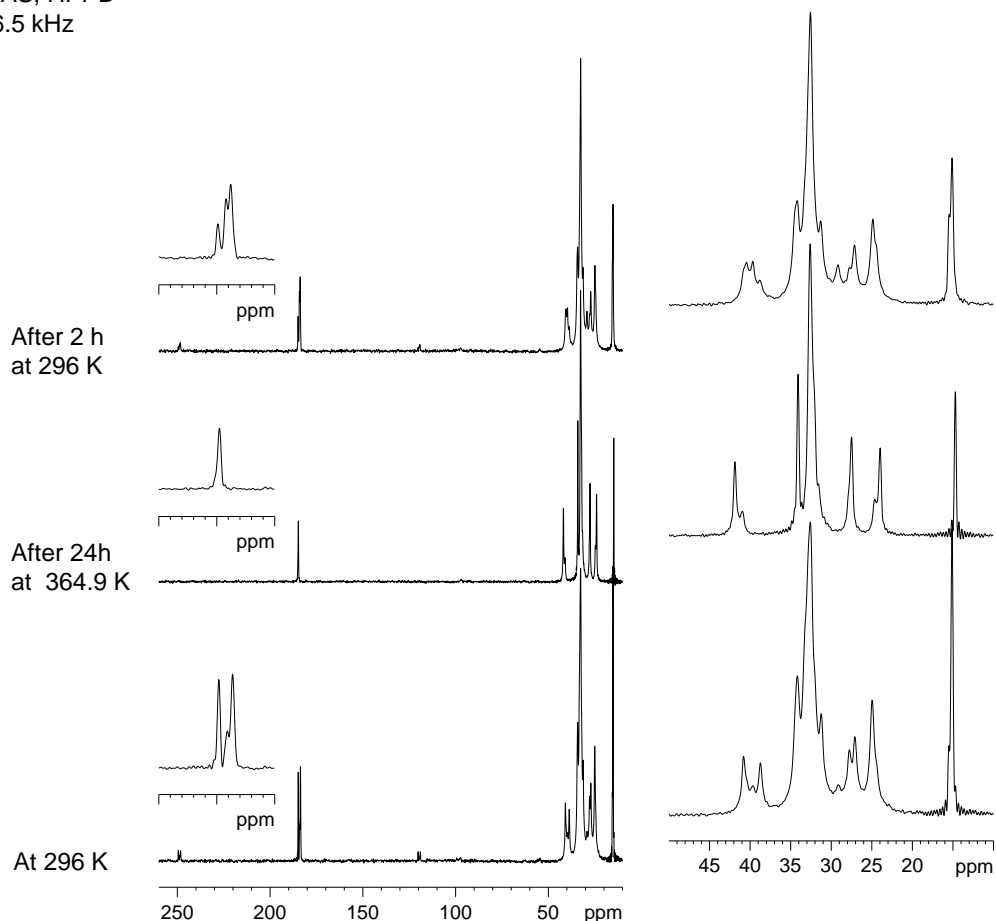


**Fig. S17.** C-13 ssNMR measurements of Pb(C10)<sub>2</sub>. The chemical shifts (ppm) at 296 K are assigned as follows: C(1): 184.4 (m); C(2): 39.7 (m); C(3): 27.4 (d); C(5-8): 34.2-31.2; C(9): 24.9; and C(10): 15.5, 15.1. At 364.9, a line narrowing of all resonances is observed due to an increase in mobility. It is noteworthy to highlight the observation of one carboxyl peak C(1): 184.8 ppm and, also, one C(10) at 14.7 ppm and the gauche effect shifting this peak -0.4 ppm and that of the C(9) from 24.9 to 24.0 ppm.

$^{207}\text{Pb}$  CP-MAS, HPPD

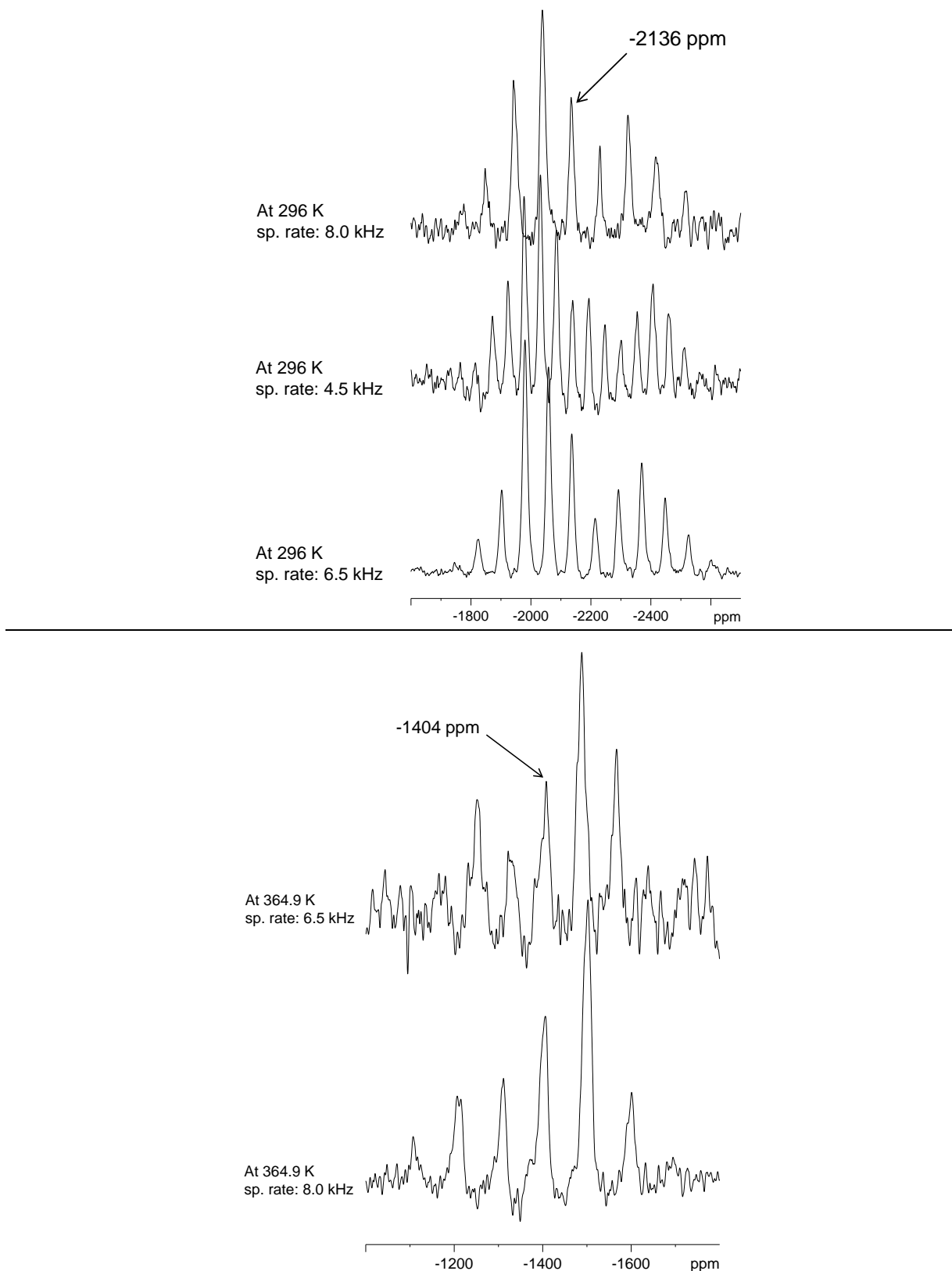


**Fig. S18.**  $\text{Pb-207}$  ssNMR measurements of  $\text{Pb}(\text{C10})_2$  at (top) 296 K and (bottom) 364.9 K.

\* Summary, NMR measurements corresponding to Pb(II) undecanoate:

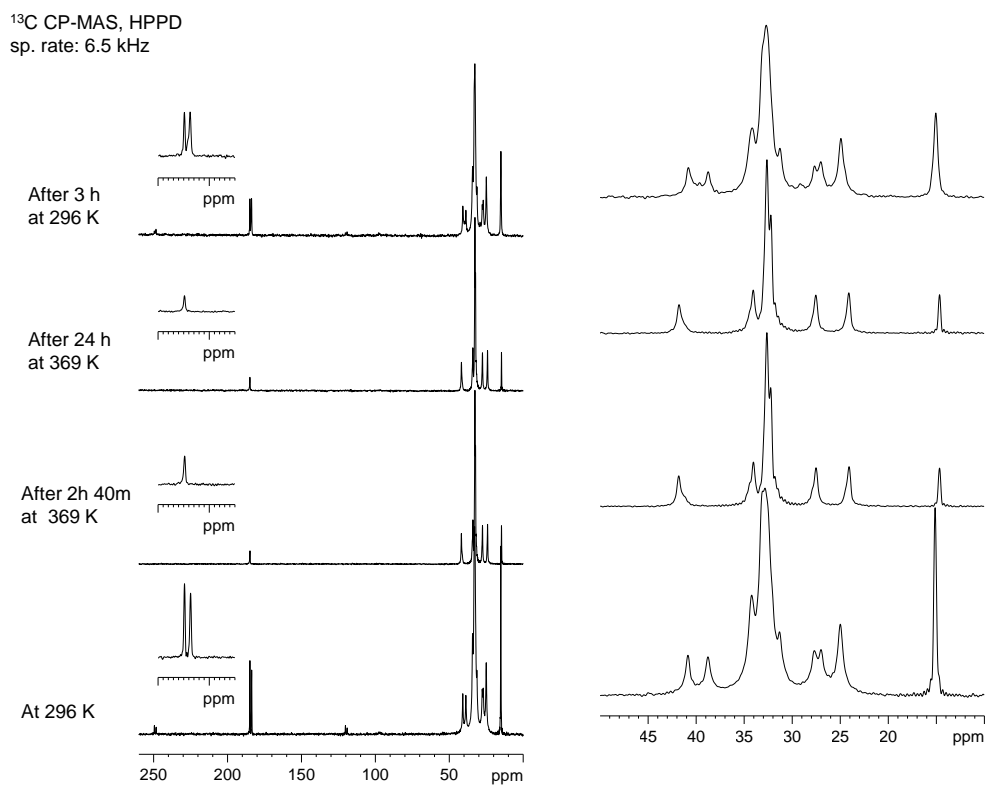


**Fig. S19.** C-13 ssNMR measurements of  $\text{Pb}(\text{C11})_2$ .

\* Summary, NMR measurements corresponding to Pb(II) tetradecanoate:

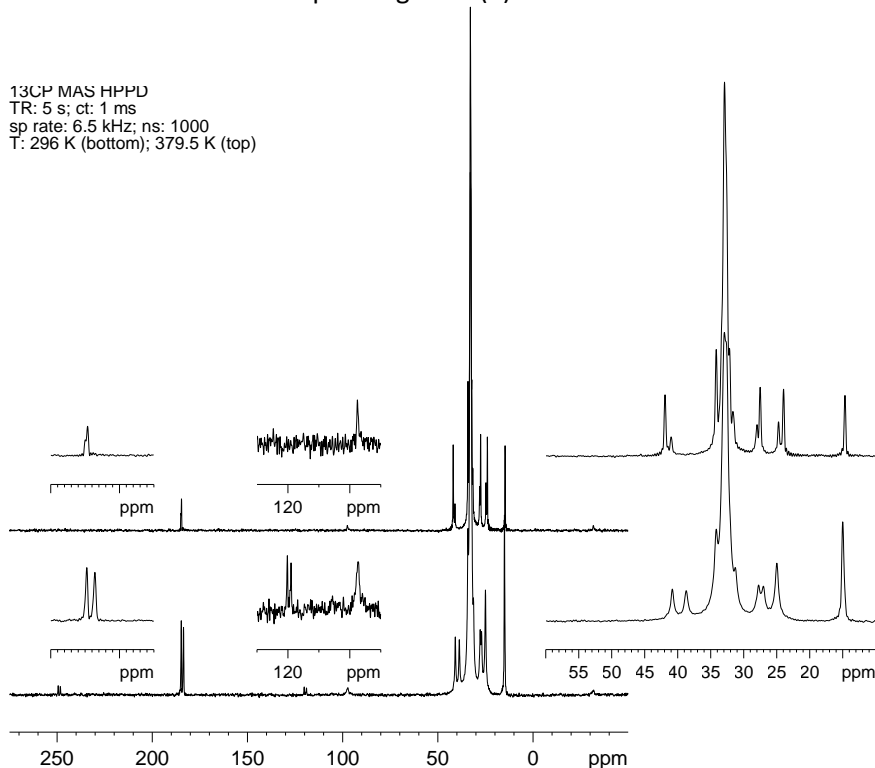


**Fig. S20.** C-13 ssNMR measurements of  $\text{Pb}(\text{C14})_2$ .

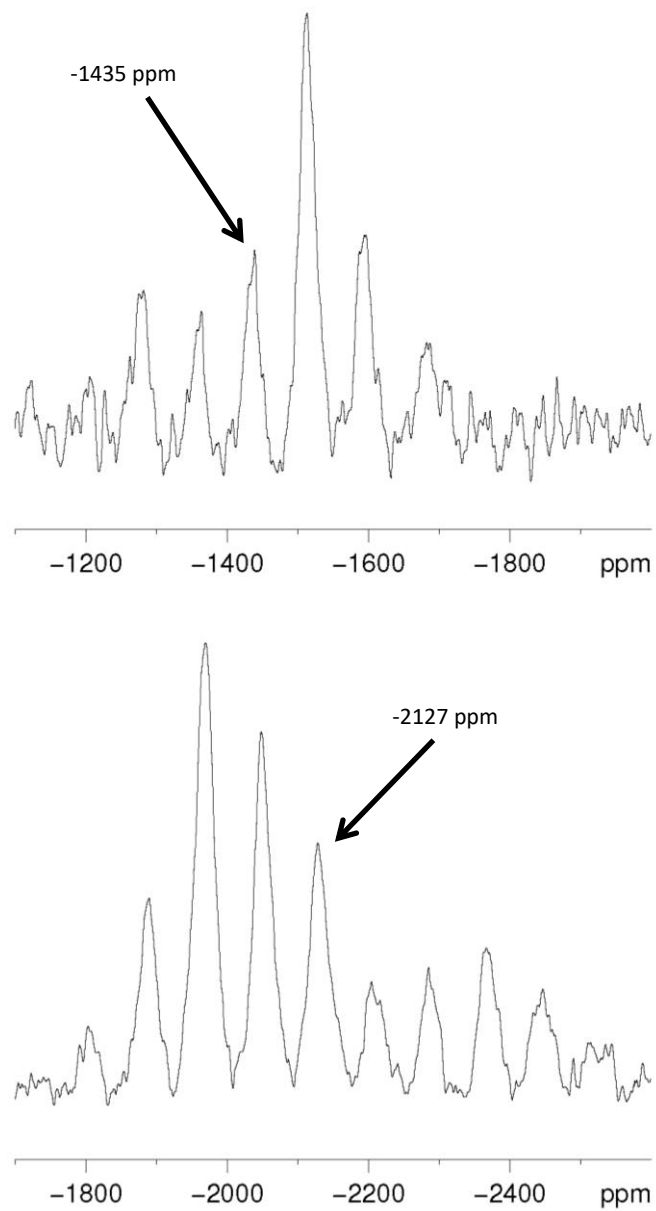


**Fig. S21.**  $\text{Pb-207}$  ssNMR measurements of  $\text{Pb(C14)}_2$  at (top) 379.5 and (bottom) 296 K.

\* Summary, NMR measurements corresponding to Pb(II) pentadecanoate:

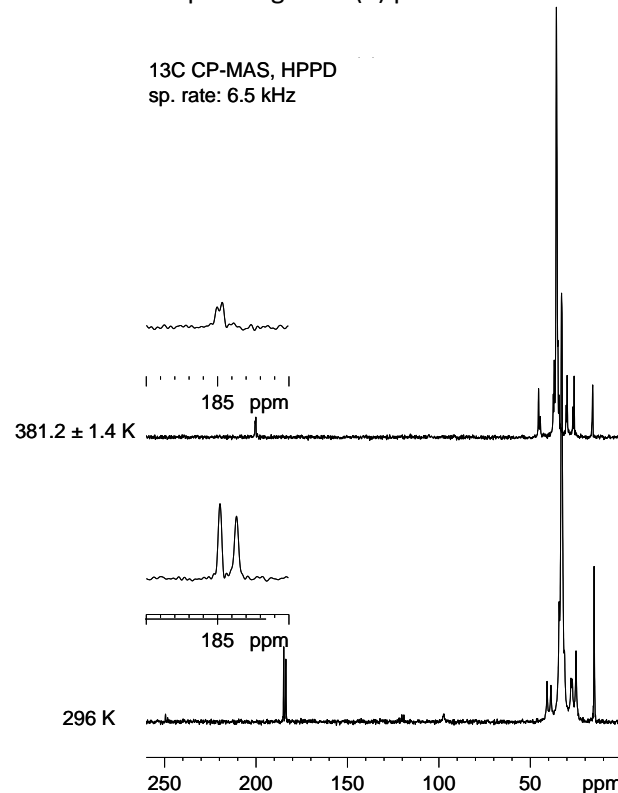


Fig. S22. C-13 ssNMR measurements of  $\text{Pb}(\text{C15})_2$ .

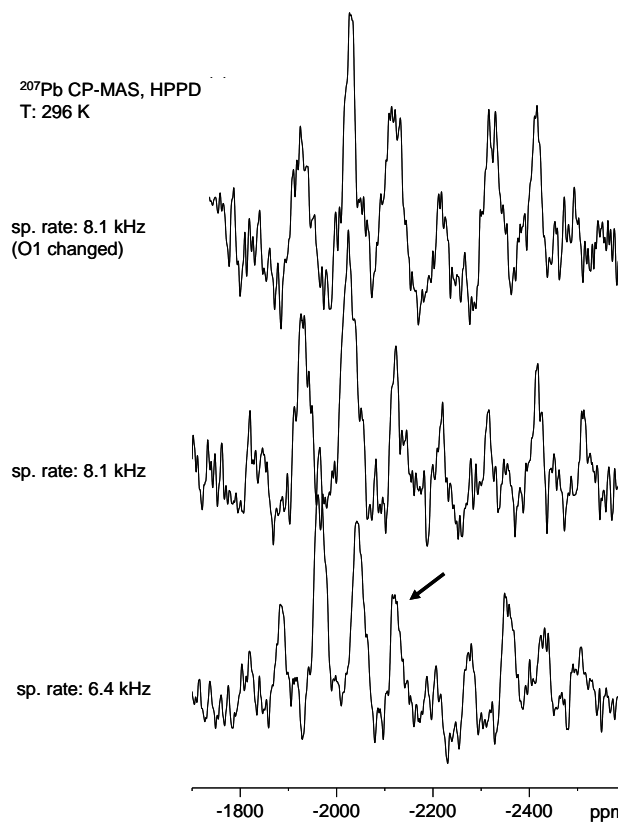


Fig. S23. Pb-207 ssNMR measurements of  $\text{Pb}(\text{C15})_2$  at 296 K.

**Table S7.** Principal components of the Pb-207 chemical shift tensors for Pb(C10)<sub>2</sub>, Pb(C11)<sub>2</sub>, Pb(C14)<sub>2</sub> and Pb(C15)<sub>2</sub>.

Compound	T (K)	$\delta_{11}$ (ppm)	$\delta_{22}$ (ppm)	$\delta_{33}$ (ppm)	$\delta_{iso}$ (ppm)	$\Omega$ (ppm)	$\kappa$
Pb(C10) <sub>2</sub>	296	-1851	-2007	-2552	-2136	700	0.55
	365	-1096	-1529	-1586	-1404	490	-0.77
Pb(C11) <sub>2</sub>	296	-1838	-1989	-2540	-2122	702	0.57
Pb(C14) <sub>2</sub>	296	-1858	-1989	-2535	-2127	677	0.61
	379	-1133	-1571	-1602	-1435	462	-0.87
Pb(C15) <sub>2</sub>	296	-1860	-1947	-2535	-2114	675	0.75

$$\delta_{iso} = (\delta_{11} + \delta_{22} + \delta_{33})/3; \Omega = |\delta_{11} - \delta_{33}|; \kappa = 3(\delta_{22} + \delta_{iso})/\Omega$$

## 8. SEM

Two different crystal morphologies were observed by SEM for  $\text{Pb}(\text{C9})_2$ .<sup>6</sup> Both types of crystals were plate-like, but they presented different angles in the planes of the plates: 90 and  $\sim 120^\circ$ . The theoretical morphology of both polymorphs, A and B, was now calculated using the Bravais, Friedel, Donnay and Harker (BFDH) algorithm (included in the *Mercury* program),<sup>7</sup> and compared to the two types of crystals observed, showing the similarities and allowing assigning the polymorphic forms to the crystals observed.

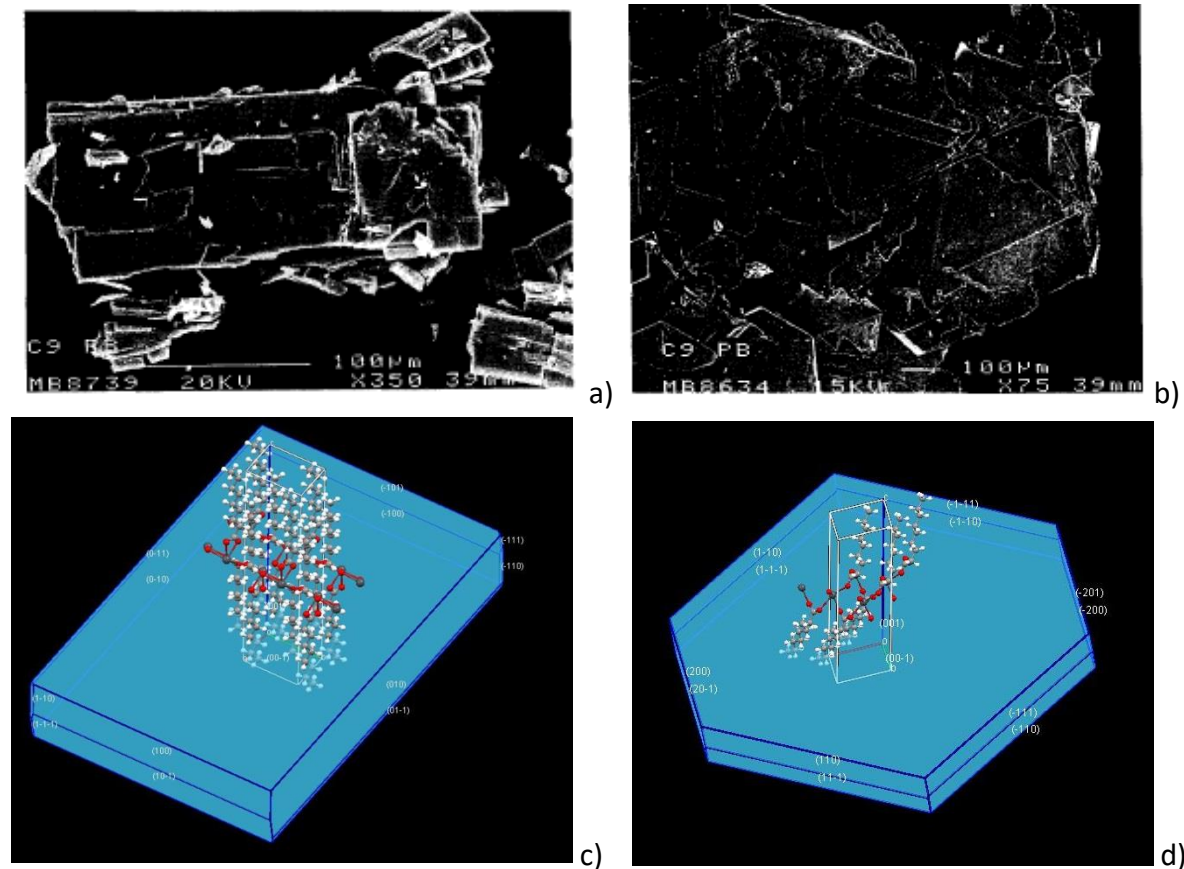


**Fig. S24.** SEM images for the two types of crystals observed for  $\text{Pb}(\text{C9})_2$  (from reference 6) (a and b) and the two theoretical morphologies assigned for the two polymorphic forms: A (c) and B (d) for the same compound.

6 M. J. González-Tejera, S. López-Andrés, M. V. García, M. I. Redondo and J. A. Rodríguez Cheda, *J. Cryst. Growth*, 1995, **152**, 330.

7 C. F. Macrae, I. J. Bruno, J. A. Chisholm, P. R. Edgington, P. McCabe, E. Pidcock, L. Rodriguez-Monge, R. Taylor, J. van de Streek, and P. A. Wood, *J. Appl. Cryst.* 2008, **41**, 466.

## 9. Structure (superstructure) of the high temperature phases in metal alkanoates

These *superstructures* were studied by Skoulios *et al.* for the high temperature phases (subwaxy, waxy, superwaxy and subneat) in alkaline soaps.<sup>8-10</sup> Thus, these superstructures are formed by the packing of domains (ribbon-like), with a dense arrangement of the polar heads in the central layers of the ribbons and a much less dense packing between ribbons, explaining the overall decrease of density with respect to the crystal phase.

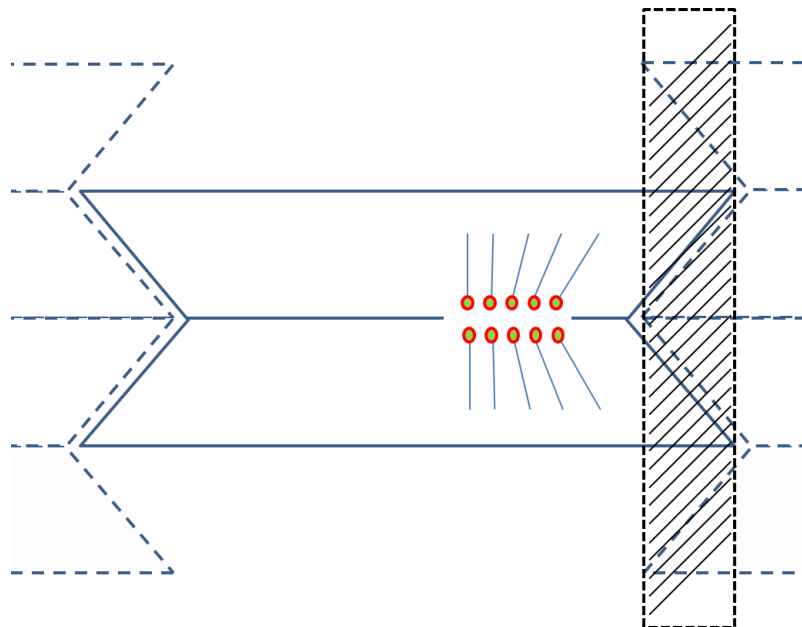


**Fig. S25.** Schematic representation of the superstructure (ribbon-like) described by Skoulios *et al.* for high temperature phases of metal soaps. The darker region represents the less dense zones (boundaries of the domains, with the tails of the alkyl chains).

8 A. E. Skoulios and V. Luzzati, *Acta Cryst.*, 1961, **14**, 278.

9 B. Gallot and A. E. Skoulios, *Acta Cryst.*, 1962, **15**, 826.

10 F. D. Gunstone, J. L. Harwood, F. B. Padley, *The Lipid Handbook*, Ed. Chapman & Hall, London, 1994